Antitumor Activity of the Selective MDM2 Antagonist Nutlin-3 Against Chemoresistant Neuroblastoma With Wild-Type p53

Tom Van Maerken, Liesbeth Ferdinande, Jasmien Taildeman, Irina Lambertz, Nurten Yigit, Liesbeth Vercruysse, Ali Rihani, Martin Michaelis, Jindrich Cinatl Jr, Claude A. Cuvelier, Jean-Christophe Marine, Anne De Paepe, Marc Bracke, Frank Speleman, Jo Vandesompele

Background Restoring p53 function by antagonizing its interaction with the negative regulator MDM2 is an appealing nongenotoxic approach to treating tumors with wild-type p53. Mutational inactivation of p53 is rare in neuroblastoma tumors at diagnosis and occurs in only a subset of multidrug-resistant neuroblastomas.

Methods The antiproliferative and cytotoxic effect of nutlin-3, a small-molecule MDM2 antagonist, was examined in chemosensitive (UKF-NB-3) and matched chemoresistant neuroblastoma cells with wild-type p53 (UKF-NB-3^{r}DOX^{20}) or with mutant p53 (UKF-NB-3^{r}VCR^{10}). Activation of the p53 pathway was assessed by expression analysis of p53 target genes, flow cytometric cell cycle analysis, and apoptosis assays. Mice with established chemoresistant tumor xenografts were treated orally with nutlin-3 or vehicle control (n = 5–10 mice per group) and were used to evaluate effects on tumor growth, p53 pathway activity, and metastatic tumor burden. All statistical tests were two-sided.

Results Nutlin-3 induced a similar activation of the p53 pathway in UKF-NB-3 and UKF-NB-3^{r}DOX^{20} cells, as evidenced by increased expression of p53 target genes, G_1 cell cycle arrest, and induction of apoptosis. No such response was observed in UKF-NB-3^{r}VCR^{10} cells with mutant p53. Oral administration of nutlin-3 to UKF-NB-3^{r}DOX^{20} xenograft–bearing mice led to inhibition of primary tumor growth (mean tumor volume after 3 weeks of treatment, nutlin-3– vs vehicle-treated mice: 772 vs 1661 mm^3, difference = 890 mm^3, 95% confidence interval = 469 to 1311 mm^3, $P < .001$), p53 pathway activation, and reduction in the extent of metastatic disease. The growth of UKF-NB-3^{r}VCR^{10} xenografts was unaffected by nutlin-3.

Conclusions Nutlin-3 activates the p53 pathway and suppresses tumor growth in this model system of chemoresistant neuroblastoma, provided that wild-type p53 is present.

J Natl Cancer Inst 2009;101:1562–1574

Neuroblastoma is the most common solid extracranial malignancy of childhood (1). Approximately half of all neuroblastoma patients are diagnosed with high-risk disease, which is associated with an overall survival rate of less than 40% (1). Acquisition of drug resistance is primarily responsible for treatment failure in these patients, because many tumors respond well to initial chemotherapy but eventually progress as intractable disease (2). Several factors are thought to contribute to the emergence of multidrug resistance in neuroblastoma. Loss of function of the gatekeeper protein p53 has been shown to confer a broad multidrug-resistant phenotype in neuroblastoma cells (3,4). Accordingly, increased frequencies of mutations in the *TP53* gene as well as aberrations that result in inappropriately increased activity of the p53 inhibitor MDM2 have been observed in neuroblastoma cell lines that were established from patients at relapse (5). Elevated expression of drug efflux pumps (eg, multidrug resistance–associated protein 1 and P-glycoprotein) (6–9) and high expression of detoxifying enzymes (such as glutathione synthetic and utilization enzymes) (10,11) have been implicated as a second group of mechanisms by which neuroblastoma cells evade therapeutic intervention. An overall imbalance between proapoptotic and survival signals might also give rise to chemotherapy resistance by diverting cell fate away from drug-induced apoptosis. Examples of mechanisms resulting in such a reduction in global apoptotic sensitivity in treatment-refractory

Affiliations of authors: Center for Medical Genetics (TVM, NY, LV, AR, ADP, FS, JV), Department of Clinical Chemistry, Microbiology and Immunology (TVM), Department of Pathology (LF, JT, CAC), and Laboratory of Experimental Cancerology (MB), Ghent University Hospital, Ghent, Belgium; Laboratory for Molecular Cancer Biology, Flanders Interuniversity Institute for Biotechnology–Ghent University (VIB-UGent), Ghent, Belgium (IL, J-CM); Zentrum der Hygiene, Institut für Medizinische Virologie, Klinikum der J.W. Goethe Universität, Frankfurt am Main, Germany (MM, JC).

Correspondence to: Tom Van Maerken, MD, Center for Medical Genetics, Ghent University Hospital, De Pintelaan 185, B-9000 Ghent, Belgium (e-mail: tom.vanmaerken@ugent.be).

See "Funding" and "Notes" following "References."

DOI: 10.1093/jnci/djp355

Advance Access publication on November 10, 2009.

neuroblastoma cells include activation of the phosphatidylinositol 3′-kinase/Akt survival pathway (12–14), overexpression of the antiapoptotic proteins survivin (15,16) and Bcl-2 (17,18), and decreased expression of death receptors such as Fas (19) and TRAILR (20). Specific defects in apoptotic effector pathways as a mechanism of drug resistance in neuroblastoma cells seem to converge at the death-inducing signaling complex, which governs the execution of the apoptotic program following engagement of cell surface death receptors (21).

Although the occurrence of p53 mutations inevitably argues for development of p53-independent therapeutic strategies or approaches that can restore the function of mutant p53, all other mechanisms of drug resistance outlined above remain amenable, in principle, to therapeutic exploitation of the p53 pathway. This notion is supported by the different modes of action of p53, with its principal ability to activate the mitochondrial apoptotic cascade providing a means for bypassing defects in death-inducing signaling complex signaling, and by the concept that induction of apoptosis relies on crossing a threshold without needing to correct for specific hyperactive survival pathways. Therapeutic utility of p53 reactivation for cancer is derived from the ontogenic requirement in tumor cells for apoptosis suppression, imposed by the stressed state of malignant cells, whereas normal cells are not sensitized to undergo apoptosis in response to p53-inducing stimuli. Several genetic studies in mouse models have demonstrated that inactivation of p53 is not only critical for tumor development but also for the maintenance of established tumors, suggesting that tumors are in a permanent state of addiction to the loss of p53 function and thus pointing to p53 as an attractive target for therapeutic intervention (22–24).

Nutlins are a class of *cis*-imidazoline derivatives that selectively disrupt the interaction between p53 and MDM2 in an enantiomer-specific manner (25). The release of p53 from negative control by MDM2 results in stabilization of p53 and direct activation of the p53 pathway, avoiding the nonspecific genotoxic damage inflicted by many classic cytotoxic drugs. We have previously reported that selective antagonism of MDM2 by nutlin-3, the best-studied member of the nutlin family, is highly effective in unleashing the antitumor potential of wild-type p53 in a panel of neuroblastoma cell lines, resulting in G_1 cell cycle arrest, apoptosis, premature cellular senescence, and neuronal differentiation (26). However, preclinical validation of the therapeutic benefit offered by experimental cancer therapeutics, such as nutlin-3, should be performed in a setting in which conventional drugs have failed and new treatment modalities are most urgently needed. To our knowledge, no studies have hitherto directly addressed whether activation of p53 by targeted inhibition of MDM2 is influenced by the acquisition of a multidrug-resistant phenotype. This study was undertaken to investigate the in vitro and in vivo antitumor activity of nutlin-3 in a model system of multidrug-resistant neuroblastoma that allows for study of treatment effects in relationship to p53 status.

CONTEXT AND CAVEATS

Prior knowledge

Survival rates of patients with high-risk neuroblastoma remain low because of resistance to conventional chemotherapeutic agents. p53 is a powerful tumor suppressor protein. Mutations in p53 that lead to its inactivation are rare in neuroblastoma. MDM2, a natural inhibitor of p53 that may have an increased activity in neuroblastoma, is a potential therapeutic target.

Study design

In vitro and in vivo analysis of the effects of the small-molecule MDM2 antagonist nutlin-3 on p53 activity and tumor growth in an established model system of multidrug-resistant neuroblastoma.

Contribution

Nutlin-3 activated the p53 pathway, irrespective of sensitivity to chemotherapeutic drugs, in neuroblastoma cells with wild-type p53 but not in cells with mutant p53. Oral administration of nutlin-3 as a single agent reduced tumor growth and metastasis in the presence of wild-type p53.

Implications

Nutlin-3 may be a viable treatment option for advanced-stage and chemoresistant neuroblastoma with wild-type p53.

Limitations

It is possible that the findings in this model system cannot be generalized to all cases of chemoresistant neuroblastoma with wild-type p53.

From the Editors

Materials and Methods

Cells and Drug Treatment

The *MYCN*-amplified cell line UKF-NB-3 was derived from bone marrow metastases of a patient with stage IV neuroblastoma who had relapsed. Chemoresistant sublines were established by long-term incubation of UKF-NB-3 cells with increasing concentrations of doxorubicin or vincristine and maintained in the presence of 20 ng/mL doxorubicin (UKF-NB-3^{r}DOX^{20}) or 10 ng/mL vincristine (UKF-NB-3^{r}VCR^{10}), as described previously (27). Solutions of doxorubicin and vincristine (both from Sigma, St Louis, MO) were prepared in water according to the manufacturer's instructions. Cells were cultured in RPMI 1640 medium supplemented with 15% fetal calf serum, 2 mM glutamine, 100 IU/mL penicillin, and 100 μg/mL streptomycin (medium and supplements from Gibco–Invitrogen, Merelbeke, Belgium) in a humidified atmosphere with 5% CO_2 at 37°C. The identity of the cell lines was verified by using array comparative genomic hybridization and short tandem repeat genotyping. Etoposide was purchased from Sigma and used according to the manufacturer's instructions. Nutlin-3 (Cayman Chemical, Ann Arbor, MI) was dissolved in absolute ethanol and stored as a 10-mM stock solution in 100-μL aliquots at −20°C. Cells were exposed to various concentrations of nutlin-3 as indicated, with the final ethanol concentration kept constant in each experiment.

Analysis of Cell Viability

UKF-NB-3, UKF-NB-3^{r}DOX^{20}, and UKF-NB-3^{r}VCR^{10} cells were seeded in duplicate wells of a 96-well plate (10^4 cells per well), incubated for 6 hours to allow them to adhere to the surface, and treated with nutlin-3 (at 0, 2, 4, 8, 16, or 32 μM) for 24, 48, or 72 hours. Cell viability was determined by using the CellTiter-Glo Luminescent Cell Viability Assay (Promega, Madison, WI). Each condition was tested in three independent experiments. Sensitivity to conventional chemotherapeutic drugs was investigated

using a modified 3-(4,5-dimethyl-2-thiazolyl)-2,5-diphenyl-2H-tetrazolium bromide (MTT) assay, as described previously (28).

Real-Time Quantitative Reverse Transcription–Polymerase Chain Reaction

Total RNA was extracted from UKF-NB-3, UKF-NB-3^{r}DOX^{20}, and UKF-NB-3^{r}VCR^{10} cells (2×10^6 cells) that had been treated with 16 μM nutlin-3 or vehicle control (ethanol) for 24 hours by using an RNeasy Mini Kit (Qiagen, Hilden, Germany), with RNase-free DNase I treatment performed on an RNA extraction spin column. After treatment with RQ1 DNase (Promega) in solution, first-strand cDNA was synthesized from 2 μg of total RNA using an iScript cDNA synthesis kit (Bio-Rad, Hercules, CA). Relative mRNA expression levels were determined by using an optimized two-step SYBR Green I real-time quantitative reverse transcription–polymerase chain reaction (RT-PCR) assay (29). Primer sequences are available in the public real-time PCR primer and probe database (RTPrimerDB; http://medgen.ugent.be/rtprimerdb/) (30,31): glyceraldehyde-3-phosphate dehydrogenase (RTPrimerDB ID No. 3); succinate dehydrogenase complex, subunit A, flavoprotein (SDHA; ID No. 7); ubiquitin C (ID No. 8); cyclin-dependent kinase inhibitor 1A (p21$^{WAF1/CIP1}$; CDKN1A; ID No. 631); BCL2-associated X protein (BAX; ID No. 814); BCL2-binding component 3 (PUMA; BBC3; ID No. 3500); tumor necrosis factor receptor superfamily, member 10b (KILLER/DR5; TNFRSF10B; ID No. 133); and mouse double minute 2 homolog (MDM2; ID No. 3499). Each real-time quantitative RT-PCR assay was validated by using an in silico assay evaluation pipeline (RTPrimerDB) to determine the specificity of the primer pair, to evaluate the secondary structure of the amplicon sequence, and to identify single-nucleotide polymorphisms in the primer-annealing region, followed by experimental evaluation of PCR specificity and efficiency by using a standard curve that consisted of six consecutive fourfold serial dilutions (from 64 ng to 62.5 pg) of reverse-transcribed high-quality control RNA for quantitative RT-PCR–based gene expression analysis (Stratagene QPCR human reference total RNA; Stratagene, La Jolla, CA) (http://medgen.ugent.be/CMGG/protocols/). PCR was performed by using a LightCycler480 (Roche, Mannheim, Germany) or an iQ5 (Bio-Rad) real-time PCR detection system in reactions of 7.5 and 15 μL, respectively, that contained 250 nM of each primer and an amount of cDNA that was equivalent to 20 ng of total RNA. Gene expression levels and PCR efficiencies, along with the SEs on the gene expression levels, were calculated by using qBase^{PLUS} 1.0 analysis software (http://www.biogazelle.com) (32), which uses a delta–quantification cycle (delta–C_q) model with PCR efficiency correction and normalization to multiple reference genes (33). Expression levels of glyceraldehyde-3-phosphate dehydrogenase, SDHA, and ubiquitin C were used for normalization. All real-time quantitative RT-PCR assays were conducted in duplicate, and four repetitions of the experiment were performed using independently prepared cDNA templates.

Immunoblot Analysis

UKF-NB-3, UKF-NB-3^{r}DOX^{20}, and UKF-NB-3^{r}VCR^{10} cells (2×10^6 cells) treated with 0 or 16 μM nutlin-3 for 24 hours were solubilized in lysis buffer (1% Triton X-100, 150 mM NaCl, 50 mM HEPES [pH 7.5], 1 mM EDTA, 2.5 mM EGTA, 1 mM NaF, 10 mM β-glycerophosphate, and protease and phosphatase inhibitor cocktails [Sigma]). Cell lysates were clarified by centrifugation at 15 300*g* for 2 minutes. Total protein (60 μg) was fractionated on a 10% sodium dodecyl sulfate–polyacrylamide gel; transferred to a Hybond-P membrane (Amersham Biosciences, Piscataway, NJ); and probed with a mouse monoclonal anti-p53 antibody (1:1000 dilution; Santa Cruz Biotechnology, Santa Cruz, CA), a mouse monoclonal anti-MDM2 antibody (1:1000 dilution; Santa Cruz Biotechnology), a mouse monoclonal anti-p21$^{WAF1/CIP1}$ antibody (1:500 dilution; Santa Cruz Biotechnology), or a mouse monoclonal anti-PARP antibody (1:2000 dilution; Cell Signaling Technology, Danvers, MA). To confirm equal loading, the membranes were incubated with stripping buffer (62.5 mM Tris, 2% sodium dodecyl sulfate, and 100 mM β-mercaptoethanol) for 15 minutes at 50°C and then probed with a mouse monoclonal anti-vinculin antibody (1:10 000 dilution; Sigma). Horseradish peroxidase–conjugated anti-mouse IgG (1:4000 dilution; Cell Signaling Technology) was used as a secondary antibody. Protein–antibody complexes were visualized using ECL Plus (Amersham Biosciences) or Immobilon Western (Millipore, Billerica, MA) chemiluminescent detection reagents followed by exposure to autoradiography film (Hyperfilm ECL; Amersham Biosciences).

Cell Cycle and Hypodiploidy Analysis

Measurements of cell cycle phase distribution and sub-G_1 DNA content were performed using a DNA Prep Reagents kit (Beckman Coulter, Miami, FL) and flow cytometric analysis. Briefly, UKF-NB-3, UKF-NB-3^{r}DOX^{20}, and UKF-NB-3^{r}VCR^{10} cells (1×10^6 cells) were seeded in a 25-cm^2 flask, cultured overnight, and treated with 16 μM nutlin-3 or vehicle control for 24 or 48 hours. The cells were detached from the substratum by incubation with trypsin–EDTA, washed with phosphate-buffered saline (PBS; 137 mM NaCl, 2.7 mM KaCl, 10 mM Na_2HPO_4, and 2 mM KH_2PO_4 [pH 7.4]), permeabilized in 100 μL of lysing and permeabilizing reagent, and incubated for 15 minutes at room temperature with 2 mL of staining solution containing 50 μg/mL propidium iodide and 4 kU/mL RNase type III-A. The cellular DNA content was measured with an FC500 flow cytometer (Beckman Coulter). The percentage of cells with sub-G_1 DNA content, which is indicative of apoptotic cell death, was determined by using CXP Analysis software version 2.2 (Beckman Coulter). The sub-G_1 population was isolated from the total cell population before cell cycle fractions (G_1, S, and G_2/M) were quantified by using MultiCycle software version 3.0 for Windows (Phoenix Flow Systems, San Diego, CA). Two independent experiments were performed.

DNA Fragmentation Assay

DNA from UKF-NB-3, UKF-NB-3^{r}DOX^{20}, and UKF-NB-3^{r}VCR^{10} cells (2×10^6 cells) treated with 0 or 16 μM nutlin-3 for 24 hours was extracted by using a Suicide Track DNA Ladder Isolation kit (Calbiochem, San Diego, CA). The DNA (1500-ng aliquots) was resolved by electrophoresis on a 1.5% agarose gel containing 0.5 μg/mL ethidium bromide and was visualized under ultraviolet light. Three independent experiments were performed.

Analysis of Caspase-3 and Caspase-7 Activity

UKF-NB-3, UKF-NB-3^{r}DOX^{20}, and UKF-NB-3^{r}VCR^{10} cells were plated in duplicate wells of a 96-well plate (10^4 cells per well),

incubated for 6 hours, and treated for 24 hours with nutlin-3 (0, 2, 4, 8, 16, or 32 μM). The combined activity of caspase-3 and caspase-7 was measured using the Caspase-Glo 3/7 Assay (Promega) with correction for cell viability. Three independent experiments were performed.

In Vivo Studies

Five-week-old female athymic nude mice (n = 30; CBy.Cg-*Foxn1*^{nu}/J strain; Charles River Laboratories, Brussels, Belgium) were inoculated subcutaneously into the right flank with 1×10^7 UKF-NB-3^{r}DOX^{20} cells (n = 20 mice) or UKF-NB-3^{r}VCR^{10} cells (n = 10 mice) that were suspended in 100 μL of Matrigel (BD Biosciences, Erembodegem, Belgium). Approximately 2 weeks later, after the establishment of subcutaneous xenograft tumors of 100–300 mm^3 in size, the mice were randomly assigned to receive either nutlin-3 or vehicle control (n = 9–10, UKF-NB-3^{r}DOX^{20}–inoculated mice per group; n = 5, UKF-NB-3^{r}VCR^{10}–inoculated mice per group). Sample sizes for UKF-NB-3^{r}DOX^{20}–inoculated mice were sufficient to detect twofold differences between treatment groups, which were allowed to have a within-group variation in tumor volume up to 50%, with a power of 80% at a statistical significance level of $\alpha = .05$. No differences in tumor volume after nutlin-3 treatment were expected in UKF-NB-3^{r}VCR^{10}–inoculated mice. Nutlin-3, prepared by custom synthesis (Cayman Chemical) and dosed at 200 mg per kg body weight in 2% Klucel and 0.2% Tween-80 (both from Fagron, Braine-l'Alleud, Belgium), or the vehicle control (2% Klucel, 0.2% Tween-80) were administered by oral gavage twice daily for 3 weeks (UKF-NB-3^{r}DOX^{20}–inoculated mice) or until euthanasia was required by a tumor size that exceeded 2000 mm^3 (UKF-NB-3^{r}VCR^{10}–inoculated mice). This dosing regimen was chosen because it was previously shown to be effective and safe in a murine osteosarcoma xenograft model (25). Dimensions of the neuroblastoma xenografts were monitored by caliper measurement three times a week, and tumor volumes were calculated using the formula $0.4 \times a \times b^2$, where a is the largest tumor diameter and b is the smallest tumor diameter. The general physical status of mice was recorded daily, and body weight measurements were performed weekly. Euthanasia was performed by cervical dislocation. Whole blood was collected by cardiac puncture, and the tumor, liver, and lungs were removed and cut into half. One piece of the tissue was snap-frozen in liquid nitrogen and stored at −80 °C, whereas the other half was fixed in buffered formalin followed by paraffin embedding.

We performed a separate experiment that was aimed at expression analysis of the p53 pathway and immunohistochemical evaluation of caspase-3 activity. CBy.Cg-*Foxn1*^{nu}/J mice with established UKF-NB-3^{r}DOX^{20} xenografts of approximately 700 mm^3 (ie, 24 days after tumor cell inoculation) were treated orally with three doses of nutlin-3 (200 mg per kg body weight) or vehicle control over a course of 24 hours (doses were given at 0, 12, and 24 hours; n = 5–6 mice per treatment group). The mice were killed by cervical dislocation 4 hours after the last dose, and their tumors were excised and cut into two pieces for snap-freezing in liquid nitrogen and fixation in buffered formalin.

All mouse studies were performed in accordance with the Council of Europe guidelines for accommodation and care of laboratory animals. Protocols were approved by the Institutional Ethical Commission for Animal Experimentation (reference number ECD 05/40).

Analysis of p53 Target Gene Expression In Vivo by Real-Time Quantitative RT-PCR

Total RNA was extracted from cryosections of UKF-NB-3^{r}DOX^{20} xenografts that had been collected from mice treated with three oral doses of 200 mg/kg nutlin-3 or vehicle control for 24 hours (n = 5–6 mice per treatment group) by using an RNeasy Mini kit (Qiagen). DNase treatment, cDNA synthesis, and real-time quantitative RT-PCR analysis for expression of p53 target genes were performed as described above. Expression levels of glyceraldehyde-3-phosphate dehydrogenase, SDHA, and ubiquitin C were used for normalization.

Immunohistochemical Analysis of Caspase-3 Activity

Paraffin-embedded sections of UKF-NB-3^{r}DOX^{20} xenografts from mice that had been treated with three oral doses of 200 mg/kg nutlin-3 or vehicle control for 24 hours were deparaffinized in xylene, followed by rehydration by transfer through a graded alcohol series. Subsequently, heat-induced antigen retrieval was performed with EDTA buffer (pH 8.0), and endogenous peroxidase activity was blocked with 0.3% hydrogen peroxide in PBS. After washing with PBS, nonspecific binding sites were blocked with 1% bovine serum albumin in PBS. The sections were then incubated for 1 hour with a rabbit polyclonal anti-human antibody against active caspase-3 (1:1000 dilution; R&D Systems, Minneapolis, MN), rinsed, and exposed to biotinylated swine anti-rabbit secondary antibody (1:400 dilution; Dako, Glostrup, Denmark) for 30 minutes. After a further washing step, the sections were incubated with horseradish peroxidase–conjugated streptavidin (1:300 dilution; Dako) for 30 minutes. The slides were washed with PBS, and color was developed using 3-amino-9-ethylcarbazole (Dako). Finally, the sections were counterstained with hematoxylin and mounted under glass coverslips with Aquatex (Merck, Darmstadt, Germany). Specificity of staining was ensured by inclusion of a negative control section in which the primary antibody was substituted by irrelevant rabbit Igs (1:800 dilution; Santa Cruz Biotechnology). Caspase-3–positive cells, defined as cells with red staining of the cytoplasm and scored in a blinded manner, were quantified by averaging 10 high-power fields (×400 magnification) per tumor, avoiding areas of necrosis, for all individual mice (n = 5–6 mice in each treatment group). Results are expressed as mean number of caspase-3–positive cells per high-power field.

Evaluation of Metastatic Disease by Real-Time Quantitative PCR and RT-PCR

For real-time quantitative PCR–based assessment of metastatic disease in mice carrying UKF-NB-3^{r}DOX^{20} xenografts after 3 weeks of twice daily oral treatment with 200 mg/kg nutlin-3 or vehicle control, genomic DNA was isolated from approximately 20 cryosections of liver and lungs (n = 6 DNA samples for each organ site per treatment group) by using a QIAamp DNA Mini kit (Qiagen) and from blood samples (n = 4–6 DNA samples per group) by using a QIAamp DNA Blood Mini kit (Qiagen). Copy number levels were determined for the human *MYCN* gene and

for the murine *Hprt1* and *Pthlh* genes. Primer sequences are available in RTPrimerDB (http://medgen.ugent.be/rtprimerdb/) (30,31): v-myc avian myelocytomatosis viral–related oncogene, neuroblastoma-derived (*MYCN*; RTPrimerDB ID No. 11), hypoxanthine guanine phosphoribosyl transferase 1 (*Hprt1*; ID No. 45), and parathyroid hormone–like peptide (*Pthlh*; ID No. 3314). Real-time quantitative PCR with SYBR Green I detection chemistry and qBase^{PLUS} 1.0 analysis were performed as described above for quantification of mRNA expression levels, except that we used 10 ng of genomic DNA as template for the PCR reaction and *Hprt1* and *Pthlh* as the reference genes for normalization.

In parallel, total RNA was extracted from liver and lungs of UKF-NB-3^{r}DOX^{20} xenograft–bearing mice that had been treated orally with 200 mg/kg nutlin-3 or vehicle control twice daily for 3 weeks by using an RNeasy Mini kit (Qiagen) (n = 6 RNA samples, each derived from approximately 20 cryosections, for each organ site per treatment group). Residual DNA was removed by DNase treatment, cDNA was synthesized, and real-time quantitative RT-PCR analysis was performed as described above. Expression levels were determined for the human *MYCN* gene and for the murine *Ppia*, *Tbp*, and *Ubc* genes. Primer sequences are available in RTPrimerDB (http://medgen.ugent.be/rtprimerdb/) (30,31): MYCN (RTPrimerDB ID No. 180), peptidylprolyl isomerase A (Ppia; ID No. 3310), TATA box–binding protein (Tbp; ID No. 3877), and ubiquitin C (Ubc; ID No. 3874). Levels of Ppia, Tbp, and Ubc expression were used for normalization of MYCN expression.

This real-time quantitative PCR and RT-PCR approach allows for estimation of the relative amount of *MYCN* DNA and the relative expression of MYCN mRNA, respectively, at a given organ site. We considered both variables to be reflective of the neuroblastoma tumor load. A comparison of these indicators between vehicle- and nutlin-3–treated mice was performed for each individual organ system and, by using a previously described standardization procedure comprising log transformation, mean centering, and autoscaling (34), across the different organ systems.

Morphological Evaluation of Metastatic Foci

Histopathologic evaluation of metastatic disease was performed in a blinded manner by an experienced pathologist on hematoxylin and eosin–stained paraffin sections of liver and lungs from mice bearing UKF-NB-3^{r}DOX^{20} xenografts after 3 weeks of twice daily oral treatment with 200 mg/kg nutlin-3 or vehicle control. Metastatic foci were defined as groups of at least three adjacent tumor cells. The frequency of metastatic foci was quantified for 10 randomly chosen microscopic fields (×200 magnification) per organ site per mouse (n = 6 evaluated mice in each treatment group) and expressed as the mean number of metastatic foci per microscopic field.

Statistical Analysis

Analysis of cell viability data was performed using GraphPad Prism software version 5.01 for Windows (GraphPad Software, San Diego, CA). The nutlin-3 concentrations that caused 50% inhibition of cell growth (IC_{50} values) and corresponding 95% confidence intervals (CIs) were computed by fitting a sigmoidal curve with variable slope to the dose–response data. The 95% confidence interval for the ratio of two IC_{50} values was determined by using the half maximal effective concentration (EC_{50}) shift equation in GraphPad Prism. Differences in the fold induction in expression level after nutlin-3 treatment between cell lines and differences in outcome measures (tumor growth, expression of p53 target genes, apoptosis, *MYCN* DNA content, MYCN mRNA expression level, and frequency of metastatic foci) between treatment groups of mice were analyzed by the nonparametric Mann–Whitney test with the use of SPSS software version 16.0 for Windows (SPSS, Chicago, IL). All statistical tests were two-sided. *P* values less than .05 were considered statistically significant.

Results

Model System of Multidrug-Resistant Neuroblastoma and Effect of Nutlin-3 on Cell Viability

To investigate the antitumor activity of nutlin-3 against multidrug-resistant neuroblastoma, we used a well-established model system of acquired drug resistance that closely resembles advanced-stage neuroblastoma. Long-term exposure of human neuroblastoma UKF-NB-3 cells to gradually increasing concentrations of doxorubicin or vincristine resulted in the generation of sublines, designated as UKF-NB-3^{r}DOX^{20} and UKF-NB-3^{r}VCR^{10}, respectively, that were profoundly resistant to a variety of chemotherapeutic agents and γ-irradiation and that displayed, compared with the parental UKF-NB-3 cells, increased survival in serum-free medium, increased proliferative and invasive capacity, and enhanced tumorigenicity (35,36). Overexpression of P-glycoprotein and constitutive phosphorylation of Akt contribute to the chemoresistant and increased survival phenotype, respectively, of both sublines (35), and decreased expression of the NCAM (CD56) adhesion receptor might cause the enhanced invasive potential of UKF-NB-3^{r}VCR^{10} cells (36). UKF-NB-3^{r}DOX^{20} cells and parental chemosensitive UKF-NB-3 cells are wild-type for p53, whereas UKF-NB-3^{r}VCR^{10} cells carry a 404G>T (C135F) missense mutation in the *TP53* gene (35). In contrast to the abundant overexpression of P-glycoprotein in UKF-NB-3^{r}DOX^{20} and UKF-NB-3^{r}VCR^{10} cells, gene expression levels of other proteins involved in the extrusion of toxic substances from cells, such as MRP1, MRP2, and LRP, are comparable to those in UKF-NB-3 cells (data not shown). Qualitative information on phenotypically relevant genes and the IC_{50} values for some chemotherapeutic drugs commonly used to treat neuroblastoma are represented in Table 1.

Targeted inhibition of the p53–MDM2 interaction by nutlin-3 decreased the viability of UKF-NB-3 cells in a dose- and time-dependent manner, with IC_{50} values in the low micromolar range (at 24 hours of treatment, IC_{50} = 3.62 μM, 95% CI = 3.04 to 4.33 μM; at 48 hours, IC_{50} = 2.49 μM, 95% CI = 2.23 to 2.77 μM; at 72 hours, IC_{50} = 2.03 μM, 95% CI = 1.90 to 2.16 μM) (Figure 1, A). A pronounced reduction in cell viability after treatment with nutlin-3, indicative of an antiproliferative and cytotoxic effect, was also recorded for the chemoresistant UKF-NB-3^{r}DOX^{20} cells with wild-type p53, which displayed slightly higher IC_{50} values than the parental UKF-NB-3 cells (at 24 hours, IC_{50} = 4.81 μM, 95% CI = 4.46 to 5.20 μM, 1.33-fold increase in IC_{50} compared with UKF-NB-3 cells, 95% CI = 1.09- to 1.57-fold; at 48 hours, IC_{50} = 3.55 μM, 95% CI = 3.43 to 3.68 μM, 1.43-fold increase in IC_{50}

Table 1. Characteristics of UKF-NB-3, UKF-NB-3^{r}DOX^{20}, and UKF-NB-3^{r}VCR^{10} cells*

Cell line	*MYCN*†	*TP53*‡	P-gp§	Akt§	NCAM§	Mean IC_{50}, ng/mL (95% CI)‖		
						Doxorubicin	Vincristine	Etoposide
UKF-NB-3	Amp	WT	Referent	Referent	Referent	7.3 (2.1 to 12.5)	0.3 (0 to 0.7)	116 (18 to 214)
UKF-NB-3^{r}DOX^{20}	Amp	WT	↑	↑	≡	72 (32 to 111)	199 (96 to 302)	341 (114 to 568)
UKF-NB-3^{r}VCR^{10}	Amp	404G>T (C135F)	↑	↑	↓	59 (19 to 100)	69 (37 to 100)	386 (156 to 616)

* ↑ = increased; ↓ = decreased; ≡ = unchanged; Amp = amplified; CI = confidence interval; IC_{50} = concentration resulting in 50% inhibition of cell growth; WT = wild-type.

† Genomic amplification status.

‡ Mutation status. Mutation is indicated by nucleotide change followed by amino acid change.

§ Expression level (P-gp, NCAM) or phosphorylation level (Akt) relative to parental UKF-NB-3 cells.

‖ Derived from three independent experiments, each performed in eight replicates.

compared with UKF-NB-3 cells, 95% CI = 1.28- to 1.57-fold; at 72 hours, IC_{50} = 3.14 μM, 95% CI = 3.06 to 3.22 μM, 1.55-fold increase in IC_{50} compared with UKF-NB-3 cells, 95% CI = 1.45- to 1.64-fold) (Figure 1, B). In contrast, and as expected for a cell line with mutant p53, nutlin-3 did not reduce the viability of UKF-NB-3^{r}VCR^{10} cells unless a relatively high concentration was used (at 24 hours, IC_{50} was above the upper limit of the concentration range studied [32 μM], at least an 8.83-fold increase in IC_{50} compared with UKF-NB-3 cells; at 48 hours, IC_{50} = 26.08 μM, 95% CI = 22.89 to 29.73 μM, 10.49-fold increase in IC_{50} compared with UKF-NB-3 cells, 95% CI = 8.79- to 12.18-fold; at 72 hours, IC_{50} = 21.22 μM, 95% CI = 18.95 to 23.76 μM, 10.46-fold increase in IC_{50} compared with UKF-NB-3 cells, 95% CI = 9.11- to 11.81-fold) (Figure 1, C). These results indicate that neuroblastoma cells with a multidrug-resistant profile to conventional chemotherapeutic agents may remain sensitive to nutlin-3, provided that wild-type p53 is retained.

Effect of Nutlin-3 on the p53 Pathway, Cell Cycle, and Apoptosis in Neuroblastoma Cells

According to our understanding of p53 regulation by MDM2, exposure of cells with wild-type p53 to a selective antagonist of p53–MDM2 binding should result in stabilization and activation of the p53 protein, induction of expression of p53 target genes, and activation of cell cycle checkpoints and apoptotic pathways. We used a real-time quantitative RT-PCR assay to evaluate expression of p53-transactivated target genes that have been implicated in cell cycle arrest (CDKN1A [p21$^{WAF1/CIP1}$]), apoptosis (BAX, BBC3 [PUMA], and TNFRSF10B [KILLER/DR5]), and autoregulation of the p53 response (MDM2). Treatment with 16 μM nutlin-3 for 24 hours resulted in an increase in the expression of these genes in both chemosensitive UKF-NB-3 and chemoresistant UKF-NB-3^{r}DOX^{20} cells (Figure 2, A). Fold inductions in expression level after treatment with nutlin-3 were similar in UKF-NB-3 and UKF-NB-3^{r}DOX^{20} cells for the proapoptotic p53 target genes BAX (P = .149), BBC3 (P = .149), and TNFRSF10B (P = 1.0). Expression of MDM2 was increased by nutlin-3 treatment to a slightly higher extent in UKF-NB-3^{r}DOX^{20} cells than in UKF-NB-3 cells (6.08-fold increase vs 3.32-fold increase, difference = 2.76-fold increase, 95% CI = 1.78- to 3.75-fold increase, P = .021), whereas the nutlin-3–induced increase in expression of CDKN1A was somewhat more pronounced in UKF-NB-3 cells than in UKF-NB-3^{r}DOX^{20} cells (30.74-fold increase vs 9.55-fold increase, difference = 21.20-fold increase, 95% CI = 17.50- to 24.89-fold increase, P = .021). In contrast, treatment of p53-mutant UKF-NB-3^{r}VCR^{10} cells with 16 μM nutlin-3 for 24 hours did not result in an appreciable increase in expression of p53 target genes compared with vehicle-treated cells, except for a 2.53-fold (95% CI = 2.27- to 2.79-fold) increase in CDKN1A expression (Figure 2, A). As expected, fold inductions in expression level of p53 target genes after exposure to nutlin-3 were statistically significantly greater in UKF-NB-3 cells than in UKF-NB-3^{r}VCR^{10} cells (P = .021 in each case). To confirm these findings, immunoblotting was performed with primary antibodies against p53, p21$^{WAF1/CIP1}$, and MDM2 after exposure of cells to vehicle control or 16 μM nutlin-3 for 24 hours. In agreement with the previous results, treatment with nutlin-3 led to

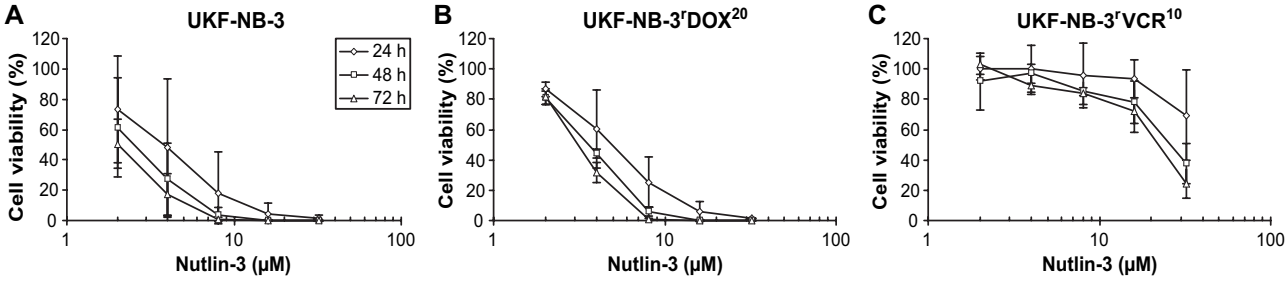

Figure 1. Effect of nutlin-3 on cell viability. Exponentially growing **A**) UKF-NB-3, **B**) UKF-NB-3^{r}DOX^{20}, and **C**) UKF-NB-3^{r}VCR^{10} cells were treated with a range of nutlin-3 concentrations (0–32 μM) for 24, 48, or 72 hours, and cell viability with respect to vehicle-treated cells was determined using the CellTiter-Glo Luminescent Cell Viability Assay. Three independent experiments were performed, each in duplicate. Mean cell viability values, derived from the means of the individual experiments (n = 3), and their 95% confidence intervals (**error bars**) are shown.

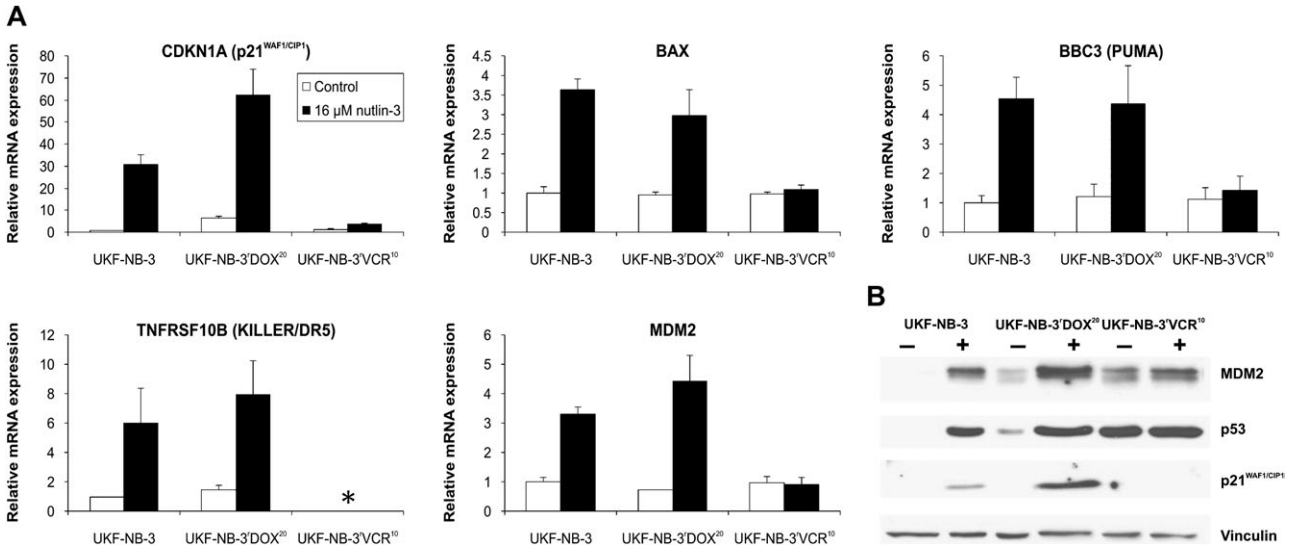

Figure 2. Effect of nutlin-3 on the expression of p53 and its target genes in UKF-NB-3, UKF-NB-3^{r}DOX^{20}, and UKF-NB-3^{r}VCR^{10} cells. **A**) Real-time quantitative reverse transcription–polymerase chain reaction analysis of expression of p53 target genes (CDKN1A [p21$^{WAF1/CIP1}$], BAX, BBC3 [PUMA], TNFRSF10B [KILLER/DR5], and MDM2) in UKF-NB-3 and UKF-NB-3^{r}DOX^{20} cells with wild-type p53 and in UKF-NB-3^{r}VCR^{10} cells with mutant p53 after exposure to vehicle control or 16 μM nutlin-3 for 24 hours. Mean mRNA expression levels relative to vehicle-treated UKF-NB-3 cells, which were derived from measurement of four independently prepared cDNA templates, and their 95% confidence intervals (**error bars**) are shown. Expression levels in vehicle-treated UKF-NB-3 cells were arbitrarily set to 1. *TNFRSF10B expression was not detectable in UKF-NB-3^{r}VCR^{10} cells(**asterisk**). **B**) Immunoblot analysis of p53, p21$^{WAF1/CIP1}$, and MDM2 expression in UKF-NB-3, UKF-NB-3^{r}DOX^{20}, and UKF-NB-3^{r}VCR^{10} cells after treatment with vehicle control (−) or 16 μM nutlin-3 (+) for 24 hours. Expression of vinculin for each lysate is shown as a loading control.

accumulation of p53 protein and increased expression of p21$^{WAF1/CIP1}$ and MDM2 in UKF-NB-3 and UKF-NB-3^{r}DOX^{20} cells but not in p53-mutant UKF-NB-3^{r}VCR^{10} cells (Figure 2, B).

We next investigated the effect of nutlin-3 on cell cycle progression and apoptosis. Incubation of UKF-NB-3 and UKF-NB-3^{r}DOX^{20} cells with 16 μM nutlin-3 for 24 hours induced accumulation of cells in G_1 phase and a reciprocal reduction of the number of cells in S phase (Figure 3, A). This nutlin-3–induced inhibition of the G_1/S transition was not observed in nutlin-3–treated UKF-NB-3^{r}VCR^{10} cells (Figure 3, A). Induction of apoptosis by nutlin-3 in UKF-NB-3 and UKF-NB-3^{r}DOX^{20} cells was demonstrated by an increase in the sub-G_1 DNA content (Figure 3, B), PARP cleavage (Figure 3, C), DNA laddering (internucleosomal DNA fragmentation) on agarose gel electrophoresis (Figure 3, D), and dose-dependent activation of caspase-3 and caspase-7 (Figure 3, E). In contrast, administration of nutlin-3 to p53-mutant UKF-NB-3^{r}VCR^{10} cells resulted only in a slight increase in caspase-3 and caspase-7 activity at the highest tested concentration of 32 μM (Figure 3, B–E).

These data confirmed the hypothesis that nutlin-3 is a selective and potent activator of the p53 pathway in neuroblastoma cells irrespective of chemosensitivity and prompted us to further explore this targeted compound in a xenograft model derived from the chemoresistant UKF-NB-3^{r}DOX^{20} and UKF-NB-3^{r}VCR^{10} cells.

Effect of Nutlin-3 on the Growth of Chemoresistant Neuroblastoma Xenografts

To assess the in vivo efficacy of nutlin-3 against established multidrug-resistant neuroblastoma tumors, UKF-NB-3^{r}DOX^{20} or UKF-NB-3^{r}VCR^{10} cells were inoculated subcutaneously into the right flank of athymic nude mice and allowed to grow to tumors of 100–300 mm^3, and the mice were then treated with nutlin-3 or vehicle control. Nutlin-3 was administered by oral gavage at a dose of 200 mg/kg twice daily, with an intention to treat for 3 weeks. This treatment regimen was well tolerated and did not induce alterations in the physical status or behavior of mice, weight loss, visible abnormalities at necropsy, or any other obvious signs of toxicity. The growth of UKF-NB-3^{r}DOX^{20} xenografts was suppressed in mice that were treated with nutlin-3 (n = 9) compared with mice that were treated with vehicle control (n = 10) (Figure 4, A). At completion of the 3-week treatment course, the mean volumes of UKF-NB-3^{r}DOX^{20} xenografts were 772 mm^3 for nutlin-3–treated mice and 1661 mm^3 for vehicle-treated mice (difference in mean tumor volume between treatment groups = 890 mm^3, 95% CI = 469 to 1311 mm^3, P < .001). In contrast, and consistent with the mutant p53 status of the UKF-NB-3^{r}VCR^{10} cells, growth of UKF-NB-3^{r}VCR^{10} xenografts in nutlin-3–treated mice (n = 5) was indistinguishable from that in vehicle-treated mice (n = 5) (Figure 4, B). Mean tumor volumes in UKF-NB-3^{r}VCR^{10} xenograft–bearing mice at euthanasia, which was performed 12 days after start of the treatment course because of rapidly growing tumors, were 2057 mm^3 for nutlin-3–treated mice and 1978 mm^3 for vehicle-treated mice (difference in mean tumor volume between treatment groups = 79 mm^3, 95% CI = −968 to 1127 mm^3, P = .251).

Effect of Nutlin-3 on the p53 Pathway and Apoptosis in UKF-NB-3^{r}DOX^{20} Xenograft Tumors

We next examined whether the antitumor activity of nutlin-3 against UKF-NB-3^{r}DOX^{20} xenografts was mediated by activation of the p53 pathway. For this purpose, mice with established UKF-NB-3^{r}DOX^{20} xenografts of approximately 700 mm^3 were treated

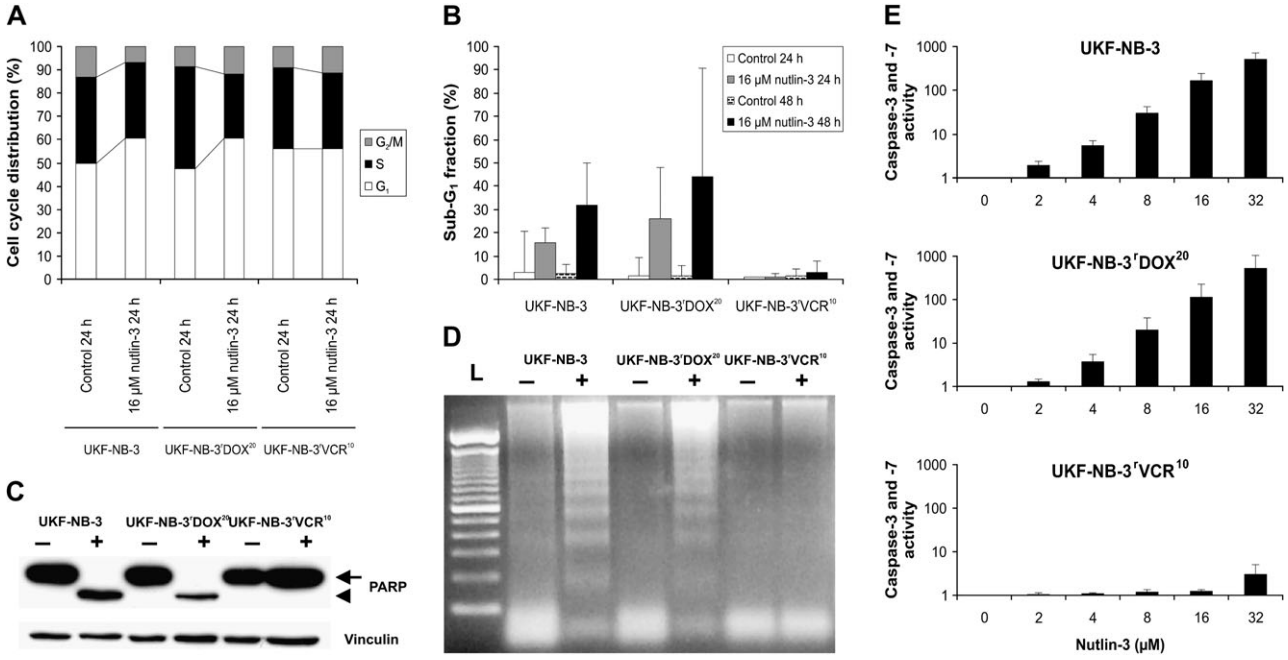

Figure 3. Effect of nutlin-3 on cell cycle progression and apoptosis of UKF-NB-3, UKF-NB-3^{r}DOX^{20}, and UKF-NB-3^{r}VCR^{10} cells. **A**) Flow cytometric analysis of cell cycle phase distribution of UKF-NB-3 and UKF-NB-3^{r}DOX^{20} cells with wild-type p53 and of UKF-NB-3^{r}VCR^{10} cells with mutant p53 after treatment with vehicle control or 16 μM nutlin-3 for 24 hours. Two independent experiments were performed. Results from one representative experiment are shown as the distributions of cells in the different phases of the cell cycle (G_1, S, and G_2/M). **B**) Flow cytometric analysis of sub-G_1 DNA content of UKF-NB-3, UKF-NB-3^{r}DOX^{20}, and UKF-NB-3^{r}VCR^{10} cells after exposure to vehicle control or 16 μM nutlin-3 for 24 and 48 hours. A nutlin-3–induced increase in sub-G_1 DNA content, indicative of apoptotic cell death, was present in UKF-NB-3 and UKF-NB-3^{r}DOX^{20} cells but not in UKF-NB-3^{r}VCR^{10} cells. The mean sub-G_1 fractions from two independent experiments, relative to the total cell population, and their 95% confidence intervals (**error bars**) are shown. **C**) Immunoblot analysis of PARP cleavage in UKF-NB-3, UKF-NB-3^{r}DOX^{20}, and UKF-NB-3^{r}VCR^{10} cells after incubation with vehicle control (−) or 16 μM nutlin-3 (**+**) for 24 hours. Cleavage of PARP, a hallmark of apoptosis, was evident after nutlin-3 treatment in UKF-NB-3 and UKF-NB-3^{r}DOX^{20} cells but not in UKF-NB-3^{r}VCR^{10} cells. Vinculin was used as a loading control. **Arrow** indicates full-length (116 kDa) PARP protein; **arrowhead** indicates the large fragment (89 kDa) of PARP resulting from caspase cleavage. **D**) Agarose gel electrophoresis of DNA extracted from UKF-NB-3, UKF-NB-3^{r}DOX^{20}, and UKF-NB-3^{r}VCR^{10} cells following exposure to vehicle control (−) or 16 μM nutlin-3 (**+**) for 24 hours. Treatment with nutlin-3 resulted in the appearance of a DNA ladder, which is characteristic of apoptosis, in UKF-NB-3 and UKF-NB-3^{r}DOX^{20} cells. No DNA fragmentation was observed after nutlin-3 treatment of UKF-NB-3^{r}VCR^{10} cells. **L** indicates a 50-base pair ladder. A representative gel image from one of three independent experiments is shown. **E**) Combined caspase-3 and caspase-7 activity in UKF-NB-3, UKF-NB-3^{r}DOX^{20}, and UKF-NB-3^{r}VCR^{10} cells after exposure to a range of nutlin-3 concentrations (0–32 μM) for 24 hours, relative to a similar amount of viable vehicle-treated cells. Three independent experiments were performed, each in duplicate. Mean combined caspase-3 and caspase-7 activity values (expressed in arbitrary units, with values in vehicle-treated cells set to 1), derived from the means of the individual experiments (n = 3), and their 95% confidence intervals (**error bars**) are shown.

with three oral doses of 200 mg/kg nutlin-3 (n = 6) or vehicle control (n = 5) for 24 hours, and tumors were analyzed for the expression of p53 target genes by real-time quantitative RT-PCR. We observed a statistically significant increase in the expression of all five evaluated p53 target genes in UKF-NB-3^{r}DOX^{20} xenografts from mice treated with nutlin-3 compared with those from vehicle-treated mice. Fold inductions in expression level after treatment with nutlin-3 compared with vehicle control were 10.05-fold (95% CI = 5.09- to 15.02-fold, $P = .006$) for CDKN1A, 1.76-fold (95% CI = 1.08- to 2.45-fold, $P = .006$) for BAX, 3.31-fold (95% CI = 1.97- to 4.66-fold, $P = .006$) for BBC3, 2.53-fold (95% CI = 1.09- to 3.96-fold, $P = .011$) for TNFRSF10B, and 1.76-fold (95% CI = 1.19- to 2.34-fold, $P = .011$) for MDM2 (Figure 5, A). Induction of apoptosis in the nutlin-3–treated

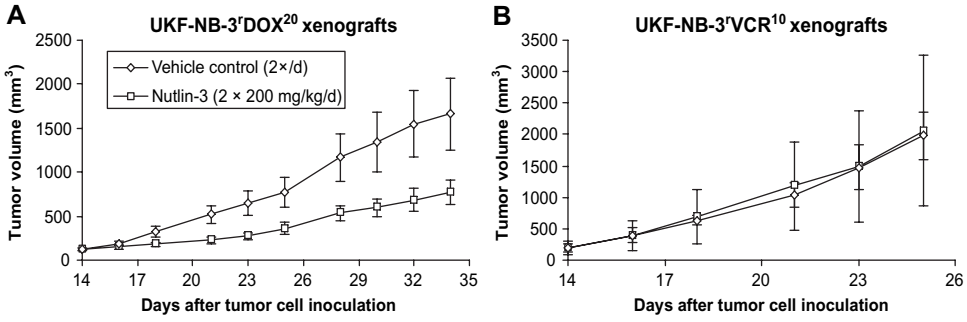

Figure 4. Effect of nutlin-3 on the growth of chemoresistant neuroblastoma xenografts. Athymic nude mice bearing established subcutaneous UKF-NB-3^{r}DOX^{20} xenografts with wild-type p53 (**A**, n = 9–10 mice per treatment group) or UKF-NB-3^{r}VCR^{10} xenografts with mutant p53 (**B**, n = 5 mice per treatment group) were treated twice daily with an oral dose of 200 mg/kg nutlin-3 or vehicle control for the period indicated, and volumes of the tumor xenografts were monitored periodically by caliper measurement. Mean tumor volumes and their 95% confidence intervals (**error bars**) are shown.

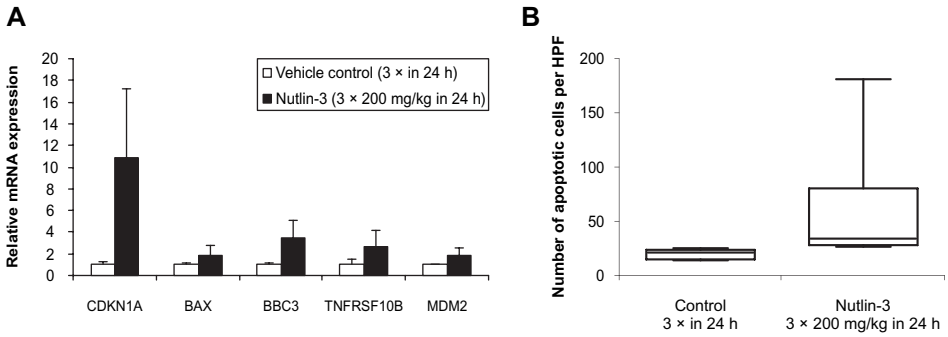

Figure 5. Effect of nutlin-3 on the p53 pathway and apoptosis in UKF-NB-3^{r}DOX^{20} xenograft tumors. **A**) Real-time quantitative reverse transcription–polymerase chain reaction analysis of expression of p53 target genes (CDKN1A [p21$^{WAF1/CIP1}$], BAX, BBC3 [PUMA], TNFRSF10B [KILLER/DR5], and MDM2) in UKF-NB-3^{r}DOX^{20} xenografts from mice that were treated orally with three doses of 200 mg/kg nutlin-3 or vehicle control for 24 hours (n = 5–6 mice per group). Mean mRNA expression levels relative to vehicle-treated mice and their 95% confidence intervals (**error bars**) are shown. Expression levels in vehicle-treated mice were arbitrarily set to 1. **B**) Immunohistochemical analysis of caspase-3 activity in sections of UKF-NB-3^{r}DOX^{20} xenografts from mice treated with three oral doses of 200 mg/kg nutlin-3 or vehicle control for 24 hours (n = 5–6 mice per group). Results are depicted as the number of caspase-3–positive cells, defined as cells with red staining of the cytoplasm, per high-power field (HPF, ×400 magnification), which was obtained for each individual tumor by averaging 10 blindly scored HPFs. For each treatment group, the median (**horizontal line**), the interquartile range (**box**), and the upper and lower range of the data (**whiskers**) are shown.

UKF-NB-3^{r}DOX^{20} xenografts was confirmed by immunohistochemical evaluation of caspase-3 activity (mean number of caspase-3–positive cells per high-power field after 24 hours of treatment, nutlin-3– vs vehicle-treated mice: 34.0 vs 19.7, difference = 14.3, 95% CI = 4.7 to 24.0, P = .006) (Figure 5, B).

Effect of Nutlin-3 on Metastatic Disease in UKF-NB-3^{r}DOX^{20} Xenograft–Bearing Mice

Finally, we examined the antitumor activity of nutlin-3 against metastatic neuroblastoma lesions in mice with established UKF-NB-3^{r}DOX^{20} xenografts. To assess metastatic tumor burden, we extracted genomic DNA from liver, lungs, and whole blood of UKF-NB-3^{r}DOX^{20} xenograft–bearing mice that had received 3 weeks of twice daily oral treatment with 200 mg/kg nutlin-3 or vehicle control and used it to perform real-time quantitative PCR (n = 4–6 mice per treatment group). We used the gene copy number of the human *MYCN* gene as an indicator of metastatic tumor load. Copy number levels of the murine *Hprt1* and *Pthlh* genes were used for normalization, allowing a quantitative comparison of tumor burden by means of the relative amount of *MYCN* DNA. Compared with vehicle-treated mice, mice treated with nutlin-3 had non–statistically significantly reduced levels of *MYCN* DNA in liver (P = .078), lungs (P = .078), and peripheral blood (P = .088) (Figure 6, A). Because elevations in *MYCN* DNA content in these organ systems represent three independent manifestations of increasing metastatic tumor burden, we next performed a pooled analysis of these data by using a standardization method (34) that allows one to draw statistically reliable conclusions on real-time quantitative PCR datasets that have different biological backgrounds. Application of this standardization procedure, which is based on log transformation, mean centering, and autoscaling, revealed a statistically significant reduction in the relative amount of *MYCN* DNA across the different organ systems of mice treated with nutlin-3 compared with those of mice treated with vehicle control (P = .002). A caveat in interpreting these results in terms of metastatic tumor burden relates to observations of circulating *MYCN* DNA in the serum of patients with *MYCN*-amplified neuroblastoma (37,38). To exclude the possibility that the nutlin-3–induced reduction in *MYCN* DNA content of liver and lungs was caused by a decrease in circulating *MYCN* DNA in these highly vascularized organs and not by a genuine effect on metastatic tumor load, we next evaluated the MYCN mRNA expression levels in liver and lungs by real-time quantitative RT-PCR. Expression levels of the murine *Ppia*, *Tbp*, and *Ubc* genes were used for normalization. UKF-NB-3^{r}DOX^{20} xenograft–bearing mice treated twice daily with 200 mg/kg nutlin-3 for 3 weeks had decreased expression of human MYCN mRNA in liver (P = .006) and lungs (P = .037) compared with mice treated with vehicle control (n = 6 mice per treatment group) (Figure 6, B), indicating that nutlin-3 had antitumor activity against metastatic lesions. A pooled analysis of the MYCN mRNA expression data from both organ sites further supported the potential value of nutlin-3 in treating metastatic neuroblastoma disease, as nutlin-3 was highly efficacious in reducing MYCN mRNA expression across both organ systems compared with vehicle control (P = .001).

Confirmation of these results was obtained by morphological evaluation of metastatic disease on hematoxylin and eosin–stained sections of liver and lungs from UKF-NB-3^{r}DOX^{20} xenograft–bearing mice. Mice treated with nutlin-3 had fewer metastatic foci, defined as groups of at least three adjacent tumor cells, in both liver and lungs compared with mice treated with vehicle control (n = 6 mice per treatment group) (Figure 6, C). In the liver sections, the mean number of metastatic foci per microscopic field at ×200 magnification was 0.17 for nutlin-3–treated mice and 0.60 for vehicle-treated mice (difference in mean number of hepatic metastatic foci per microscopic field between treatment groups = 0.43, 95% CI = 0.07 to 0.80, P = .014). In the lung sections, the mean number of metastatic foci per microscopic field at ×200 magnification was 4.85 after nutlin-3 treatment compared with 9.80 after vehicle treatment (difference in mean number of pulmonary metastatic foci per microscopic field between treatment groups = 4.96, 95% CI = 0.87 to 9.05, P = .025). These results further strengthen the concept that nutlin-3 may represent a viable treatment option for patients with advanced-stage and chemoresistant neuroblastoma with wild-type p53.

Discussion

Acquisition of a multidrug-resistant phenotype during chemotherapy represents a major hurdle to the successful treatment of

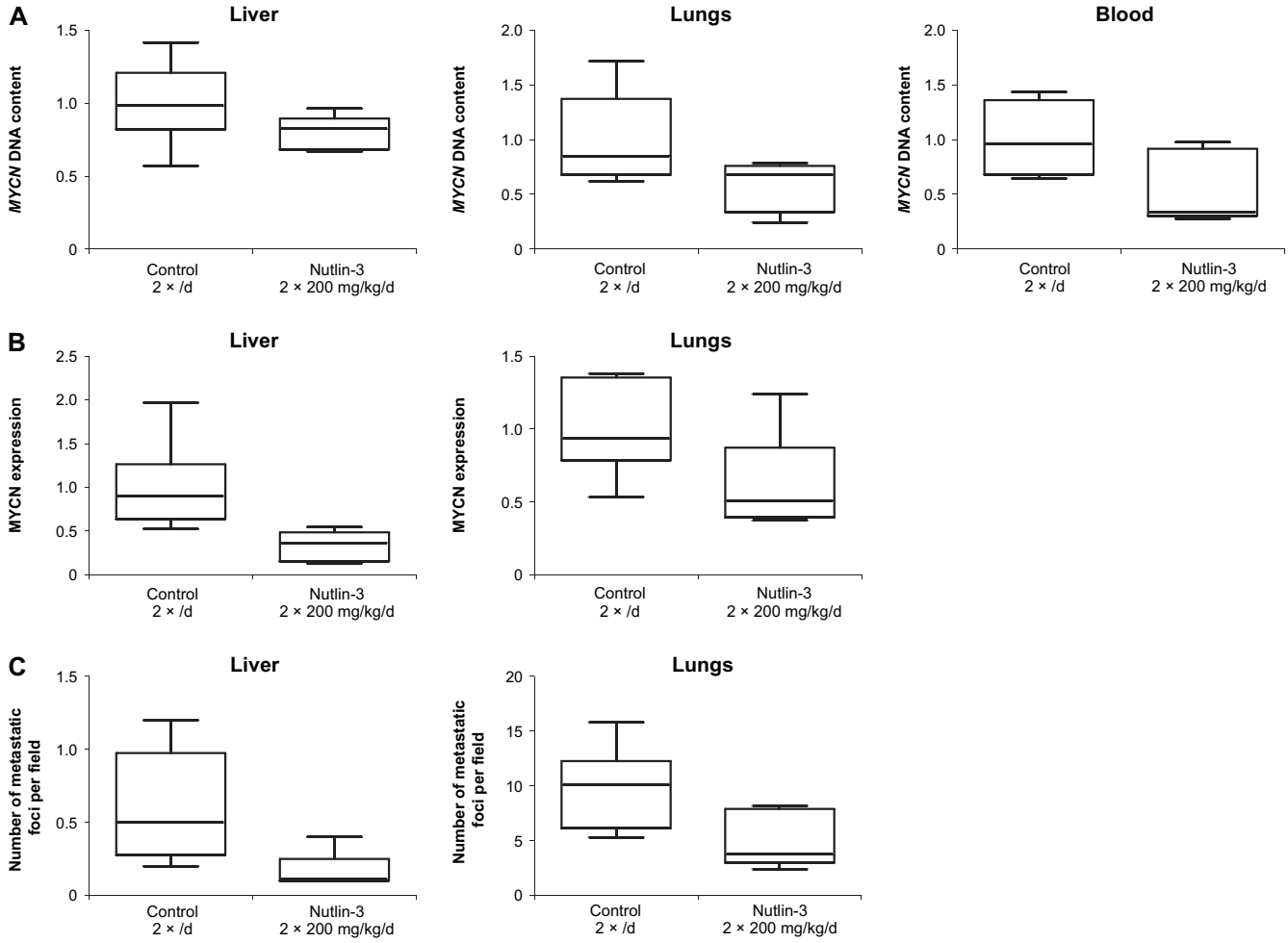

Figure 6. Effect of nutlin-3 on metastatic disease in UKF-NB-3^{r}DOX^{20} xenograft–bearing mice. **A**) Assessment of tumor burden at distant organ sites by real-time quantitative polymerase chain reaction (PCR). Mice with established UKF-NB-3^{r}DOX^{20} xenografts were treated twice daily with an oral dose of 200 mg/kg nutlin-3 or vehicle control for 3 weeks. Mice were then killed, and human *MYCN* DNA in liver, lungs, and whole blood was measured by using real-time quantitative PCR (n = 4–6 mice per group). Copy number levels of the murine *Hprt1* and *Pthlh* genes were used for normalization, allowing to compare tumor burden by means of the relative amount of *MYCN* DNA. For each organ site, the mean *MYCN* DNA content that was observed after vehicle treatment was arbitrarily set to 1. **B**) Assessment of metastatic tumor load in liver and lungs by real-time quantitative reverse transcription–PCR. The mRNA expression levels of human MYCN were measured in liver and lungs from UKF-NB-3^{r}DOX^{20} xenograft–bearing mice after oral treatment with 200 mg/kg nutlin-3 or vehicle control twice daily for 3 weeks (n = 6 mice per group). Expression levels of the murine *Ppia*, *Tbp*, and *Ubc* genes were used for normalization, allowing to compare metastatic tumor load by means of the relative expression of MYCN mRNA. For each organ site, the mean MYCN mRNA expression level that was observed after vehicle treatment was arbitrarily set to 1. **C**) Histopathologic analysis of metastatic foci in liver and lung sections from mice with UKF-NB-3^{r}DOX^{20} xenografts after 3 weeks of oral treatment with 200 mg/kg nutlin-3 or vehicle control twice daily (n = 6 mice per group). Results are expressed as the number of metastatic foci per microscopic field, which was obtained for each examined organ by averaging 10 blindly scored microscopic fields (×200 magnification). In **A**–**C**, the median (**horizontal line**), the interquartile range (**box**), and the upper and lower range of the data (**whiskers**) are shown.

neuroblastoma. Development of novel antitumor strategies is essential to improve the poor survival rates of high-risk patients (1). In this study, we evaluated the antitumor efficacy of nutlin-3, a potent and selective antagonist of the p53–MDM2 interaction, in a model system of multidrug-resistant neuroblastoma. Selection of the chemoresistant UKF-NB-3^{r}DOX^{20} and UKF-NB-3^{r}VCR^{10} sublines was achieved by long-term exposure of the parental chemosensitive UKF-NB-3 cells to cytotoxic drug doses in the range of clinical plasma concentrations and was associated with the acquisition of a spectrum of clinically relevant phenotypic characteristics, such as increased proliferative and survival capacity, enhanced invasiveness, and higher tumorigenicity (35,36). We demonstrated that treatment with nutlin-3 induces activation of the p53 pathway, G_1 cell cycle arrest, and apoptosis in chemosensitive UKF-NB-3 and chemoresistant UKF-NB-3^{r}DOX^{20} cells to a similar extent but not in UKF-NB-3^{r}VCR^{10} cells, which carry a missense mutation in the *TP53* gene. Oral administration of nutlin-3 to mice carrying established UKF-NB-3^{r}DOX^{20} xenografts was efficacious against both the primary tumor and against metastatic lesions, whereas no treatment effects were observed in UKF-NB-3^{r}VCR^{10} xenograft–bearing mice. Although these data are limited to one model system, they strongly suggest that targeted disruption of the p53–MDM2 interaction by nutlin-3 may provide a new therapeutic option for treatment of metastatic and chemorefractory neuroblastoma tumors with wild-type p53.

Important considerations in interpreting these results in terms of clinical applicability include the frequency of p53 mutations and the nature of p53-inactivating lesions in neuroblastoma, the ability to identify patients who are eligible for treatment with nutlin-3, the extent to which nutlin-3–induced p53 is fully activated, the potential toxicity of MDM2 inhibitors to normal tissues, and the possibility of secondary treatment failure because of acquisition of p53 mutations or other defects in the p53 pathway. These issues are discussed in detail in the Supplementary Data (available online). The clinical promise of the nutlin family of MDM2 antagonists for the treatment of cancer is underscored by the recent introduction of one family member, R7112, in phase I clinical trials for patients with advanced solid tumors (39) or hematologic neoplasms (40). Similarly, JNJ-26854165, a small-molecule MDM2 antagonist that targets the association of MDM2 with the proteasome rather than the p53–MDM2 interaction, is currently in clinical development (41), and it is expected that MI-219, another selective inhibitor of the p53–MDM2 interaction, will enter into clinical trials in the near future (42).

The principal goal of this study was to determine whether nutlin-3 may offer therapeutic benefit for treatment of multidrug-resistant neuroblastoma tumors that carry wild-type p53. Although we did not attempt to maximize the therapeutic response in the xenograft mouse model, it is conceivable that the actual therapeutic gain provided by nutlin-3 might extend beyond the current results. In this study, we used a racemic mixture of nutlin-3, consisting of two enantiomers with a 150-fold difference in the ability to inhibit the p53–MDM2 interaction, to treat xenograft-bearing mice according to an oral dosing regimen of 200 mg/kg twice daily for 3 weeks, a schedule that has proven to be effective and safe in a murine osteosarcoma xenograft model (25). This treatment regimen is equivalent to a 3-week oral course of the active stereoisomer nutlin-3a at a dose of 100 mg/kg twice daily. The latter scheme has been shown to retard the growth of osteosarcoma xenografts in mice, similar to our results, whereas doubling the dose to 200 mg/kg nutlin-3a twice daily for 3 weeks was capable of causing regression of the osteosarcoma tumors without inducing systemic toxicity (43).

Another important issue to consider is the potential efficacy of combining nutlin-3 with other treatment modalities. Although concurrent or subsequent administration of antimitotic drugs with nutlin-3 might result in antagonistic effects because of the ability of MDM2 inhibitors to induce a p53-dependent checkpoint arrest in tumor cells with wild-type p53 (44), several appealing opportunities for combination therapy exist. For example, intrinsic DNA damage signaling sensitizes cancer cells to nutlin-3–induced cytotoxicity (45), and many studies have reported a synergistic rather than additive interaction between nutlin-3 and genotoxic chemotherapeutics or radiotherapy [eg, (46–48)]. Interestingly, chemotherapy-induced apoptosis is also enhanced by nutlin-3a in p53-mutant cancer cells in an E2F1-dependent manner (49), suggesting that tumors with different p53 genetic backgrounds might be eligible for combinatorial regimens that incorporate nutlin compounds. A synergistic action with nutlin-3 has also been reported for gene therapeutic approaches (50) and for molecular therapeutics directed at other survival and growth-promoting pathways, including recombinant TRAIL (51), cyclin-dependent kinase inhibitors (52–54), inhibitors of the phosphatidylinositol 3′-kinase/Akt/mTOR pathway (55,56), γ-secretase inhibitors of the Notch pathway (57), a Bcl-2 family antagonist (ABT-737) (58), a pan-Aurora kinase inhibitor (MK-0457) (59), a proteasome inhibitor (bortezomib) (60), and an inhibitor of the Raf/MEK/ERK signaling cascade (PD98059) (61). However, the in vivo safety and efficacy of these combinatorial treatment strategies remains to be determined.

Some potential limitations of this study should be considered. Although the model system we have used is well established and recapitulates several clinically relevant characteristics of chemorefractory neuroblastoma tumors, it is possible that our findings cannot be extrapolated to all forms of chemoresistance in neuroblastoma. Clinical introduction of selective MDM2 antagonists will most likely take place within a combinatorial treatment setting, and this subject has not been addressed experimentally in this study. Furthermore, several issues related to the clinical translation of this novel therapeutic strategy are still unresolved, as we discuss in the Supplementary Data (available online).

In conclusion, we demonstrated that in this model system of multidrug-resistant neuroblastoma, nutlin-3 is a selective and potent activator of the p53 pathway irrespective of chemosensitivity. Oral administration of nutlin-3 as a single agent to mice with established chemorefractory neuroblastoma disease is well tolerated and effective against both primary and distant tumor sites in the presence of wild-type p53. These findings support the initiation of clinical trials of selective MDM2 antagonists for treatment of advanced-stage and chemoresistant neuroblastoma.

References

1. Maris JM, Hogarty MD, Bagatell R, Cohn SL. Neuroblastoma. *Lancet.* 2007;369(9579):2106–2120.
2. Maris JM, Matthay KK. Molecular biology of neuroblastoma. *J Clin Oncol.* 1999;17(7):2264–2279.
3. Keshelava N, Zuo JJ, Chen P, et al. Loss of p53 function confers high-level multidrug resistance in neuroblastoma cell lines. *Cancer Res.* 2001;61(16):6185–6193.
4. Xue C, Haber M, Flemming C, et al. p53 determines multidrug sensitivity of childhood neuroblastoma. *Cancer Res.* 2007;67(21):10351–10360.
5. Carr J, Bell E, Pearson AD, et al. Increased frequency of aberrations in the p53/MDM2/p14(ARF) pathway in neuroblastoma cell lines established at relapse. *Cancer Res.* 2006;66(4):2138–2145.
6. Chan HS, Haddad G, Thorner PS, et al. P-glycoprotein expression as a predictor of the outcome of therapy for neuroblastoma. *N Engl J Med.* 1991;325(23):1608–1614.
7. Norris MD, Bordow SB, Marshall GM, Haber PS, Cohn SL, Haber M. Expression of the gene for multidrug-resistance–associated protein and outcome in patients with neuroblastoma. *N Engl J Med.* 1996;334(4):231–238.
8. Blanc E, Goldschneider D, Ferrandis E, et al. MYCN enhances P-gp/MDR1 gene expression in the human metastatic neuroblastoma IGR-N-91 model. *Am J Pathol.* 2003;163(1):321–331.
9. Haber M, Smith J, Bordow SB, et al. Association of high-level MRP1 expression with poor clinical outcome in a large prospective study of primary neuroblastoma. *J Clin Oncol.* 2006;24(10):1546–1553.
10. Anderson CP, Seeger RC, Satake N, et al. Buthionine sulfoximine and myeloablative concentrations of melphalan overcome resistance in a melphalan-resistant neuroblastoma cell line. *J Pediatr Hematol Oncol.* 2001;23(8):500–505.
11. Yang B, Keshelava N, Wan Z, et al. Glutathione (GSH) and RNA expression of GSH synthetic and utilization enzymes are increased in drug-resistant neuroblastoma cell lines. *Proc Am Assoc Cancer Res.* 2003;44:1273.

12. Emran MA, Rebbaa A, Mirkin BL. Doxorubicin resistant neuroblastoma cells secrete factors that activate AKT and attenuate cytotoxicity in drug-sensitive cells. *Cancer Lett.* 2002;182(1):53–59.
13. Ho R, Eggert A, Hishiki T, et al. Resistance to chemotherapy mediated by TrkB in neuroblastomas. *Cancer Res.* 2002;62(22):6462–6466.
14. Opel D, Poremba C, Simon T, Debatin KM, Fulda S. Activation of Akt predicts poor outcome in neuroblastoma. *Cancer Res.* 2007;67(2):735–745.
15. Islam A, Kageyama H, Takada N, et al. High expression of survivin, mapped to 17q25, is significantly associated with poor prognostic factors and promotes cell survival in human neuroblastoma. *Oncogene.* 2000;19(5):617–623.
16. Azuhata T, Scott D, Griffith TS, Miller M, Sandler AD. Survivin inhibits apoptosis induced by TRAIL, and the ratio between survivin and TRAIL receptors is predictive of recurrent disease in neuroblastoma. *J Pediatr Surg.* 2006;41(8):1431–1440.
17. Dole M, Nunez G, Merchant AK, et al. Bcl-2 inhibits chemotherapy-induced apoptosis in neuroblastoma. *Cancer Res.* 1994;54(12):3253–3259.
18. Poulaki V, Mitsiades N, Romero ME, Tsokos M. Fas-mediated apoptosis in neuroblastoma requires mitochondrial activation and is inhibited by FLICE inhibitor protein and Bcl-2. *Cancer Res.* 2001;61(12):4864–4872.
19. Friesen C, Fulda S, Debatin KM. Deficient activation of the CD95 (APO-1/Fas) system in drug-resistant cells. *Leukemia.* 1997;11(11):1833–1841.
20. Yang X, Merchant MS, Romero ME, et al. Induction of caspase 8 by interferon γ renders some neuroblastoma (NB) cells sensitive to tumor necrosis factor-related apoptosis-inducing ligand (TRAIL) but reveals that a lack of membrane TR1/TR2 also contributes to TRAIL resistance in NB. *Cancer Res.* 2003;63(5):1122–1129.
21. Goldsmith KC, Hogarty MD. Targeting programmed cell death pathways with experimental therapeutics: opportunities in high-risk neuroblastoma. *Cancer Lett.* 2005;228(1–2):133–141.
22. Martins CP, Brown-Swigart L, Evan GI. Modeling the therapeutic efficacy of p53 restoration in tumors. *Cell.* 2006;127(7):1323–1334.
23. Xue W, Zender L, Miething C, et al. Senescence and tumour clearance is triggered by p53 restoration in murine liver carcinomas. *Nature.* 2007;445(7128):656–660.
24. Ventura A, Kirsch DG, McLaughlin ME, et al. Restoration of p53 function leads to tumour regression in vivo. *Nature.* 2007;445(7128):661–665.
25. Vassilev LT, Vu BT, Graves B, et al. In vivo activation of the p53 pathway by small-molecule antagonists of MDM2. *Science.* 2004;303(5659):844–848.
26. Van Maerken T, Speleman F, Vermeulen J, et al. Small-molecule MDM2 antagonists as a new therapy concept for neuroblastoma. *Cancer Res.* 2006;66(19):9646–9655.
27. Cinatl J Jr, Cinatl J, Kotchetkov R, et al. Bovine seminal ribonuclease exerts selective cytotoxicity toward neuroblastoma cells both sensitive and resistant to chemotherapeutic drugs. *Anticancer Res.* 2000;20(2A):853–859.
28. Michaelis M, Cinatl J, Anand P, et al. Onconase induces caspase-independent cell death in chemoresistant neuroblastoma cells. *Cancer Lett.* 2007;250(1):107–116.
29. Vandesompele J, De Paepe A, Speleman F. Elimination of primer–dimer artifacts and genomic coamplification using a two-step SYBR green I real-time RT-PCR. *Anal Biochem.* 2002;303(1):95–98.
30. Pattyn F, Speleman F, De Paepe A, Vandesompele J. RTPrimerDB: the real-time PCR primer and probe database. *Nucleic Acids Res.* 2003;31(1):122–123.
31. Pattyn F, Robbrecht P, De Paepe A, Speleman F, Vandesompele J. RTPrimerDB: the real-time PCR primer and probe database, major update 2006. *Nucleic Acids Res.* 2006;34(Database issue):D684–D688.
32. Hellemans J, Mortier G, De Paepe A, Speleman F, Vandesompele J. qBase relative quantification framework and software for management and automated analysis of real-time quantitative PCR data. *Genome Biol.* 2007;8(2):R19.
33. Vandesompele J, De Preter K, Pattyn F, et al. Accurate normalization of real-time quantitative RT-PCR data by geometric averaging of multiple internal control genes. *Genome Biol.* 2002;3(7):research0034.
34. Willems E, Leyns L, Vandesompele J. Standardization of real-time PCR gene expression data from independent biological replicates. *Anal Biochem.* 2008;379(1):127–129.
35. Kotchetkov R, Driever PH, Cinatl J, et al. Increased malignant behavior in neuroblastoma cells with acquired multi-drug resistance does not depend on P-gp expression. *Int J Oncol.* 2005;27(4):1029–1037.
36. Blaheta RA, Daher FH, Michaelis M, et al. Chemoresistance induces enhanced adhesion and transendothelial penetration of neuroblastoma cells by down-regulating NCAM surface expression. *BMC Cancer.* 2006;6:294.
37. Combaret V, Audoynaud C, Iacono I, et al. Circulating MYCN DNA as a tumor-specific marker in neuroblastoma patients. *Cancer Res.* 2002;62(13):3646–3648.
38. Gotoh T, Hosoi H, Iehara T, et al. Prediction of MYCN amplification in neuroblastoma using serum DNA and real-time quantitative polymerase chain reaction. *J Clin Oncol.* 2005;23(22):5205–5210.
39. Hoffmann–La Roche. A study of R7112 in patients with advanced solid tumors. In: *ClinicalTrials.gov* [Internet]. Bethesda, MD: National Library of Medicine (US); 2000. http://clinicaltrials.gov/show/NCT00559533. Accessed September 9, 2009. NLM Identifier: NCT00559533.
40. Hoffmann–La Roche. A study of R7112 in patients with hematologic neoplasms. In: *ClinicalTrials.gov* [Internet]. Bethesda, MD: National Library of Medicine (US); 2000. http://clinicaltrials.gov/show/NCT00623870. Accessed September 9, 2009. NLM Identifier: NCT00623870.
41. Johnson & Johnson Pharmaceutical Research & Development. L.L.C. A research study of JNJ-26854165 to determine the safety and dose in patients with advanced stage or refractory solid tumors. In: *ClinicalTrials.gov* [Internet]. Bethesda, MD: National Library of Medicine (US); 2000. http://clinicaltrials.gov/show/NCT00676910. Accessed September 9, 2009. NLM Identifier: NCT00676910.
42. Shangary S, Wang S. Small-molecule inhibitors of the MDM2-p53 protein-protein interaction to reactivate p53 function: a novel approach for cancer therapy. *Annu Rev Pharmacol Toxicol.* 2009;49:223–241.
43. Tovar C, Rosinski J, Filipovic Z, et al. Small-molecule MDM2 antagonists reveal aberrant p53 signaling in cancer: implications for therapy. *Proc Natl Acad Sci U S A.* 2006;103(6):1888–1893.
44. Carvajal D, Tovar C, Yang H, Vu BT, Heimbrook DC, Vassilev LT. Activation of p53 by MDM2 antagonists can protect proliferating cells from mitotic inhibitors. *Cancer Res.* 2005;65(5):1918–1924.
45. Brummelkamp TR, Fabius AW, Mullenders J, et al. An shRNA barcode screen provides insight into cancer cell vulnerability to MDM2 inhibitors. *Nat Chem Biol.* 2006;2(4):202–206.
46. Coll-Mulet L, Iglesias-Serret D, Santidrian AF, et al. MDM2 antagonists activate p53 and synergize with genotoxic drugs in B-cell chronic lymphocytic leukemia cells. *Blood.* 2006;107(10):4109–4114.
47. Barbieri E, Mehta P, Chen Z, et al. MDM2 inhibition sensitizes neuroblastoma to chemotherapy-induced apoptotic cell death. *Mol Cancer Ther.* 2006;5(9):2358–2365.
48. Cao C, Shinohara ET, Subhawong TK, et al. Radiosensitization of lung cancer by nutlin, an inhibitor of murine double minute 2. *Mol Cancer Ther.* 2006;5(2):411–417.
49. Ambrosini G, Sambol EB, Carvajal D, Vassilev LT, Singer S, Schwartz GK. Mouse double minute antagonist Nutlin-3a enhances chemotherapy-induced apoptosis in cancer cells with mutant p53 by activating E2F1. *Oncogene.* 2007;26(24):3473–3481.
50. Graat HC, Carette JE, Schagen FH, et al. Enhanced tumor cell kill by combined treatment with a small-molecule antagonist of mouse double minute 2 and adenoviruses encoding p53. *Mol Cancer Ther.* 2007;6(5):1552–1561.
51. Secchiero P, Zerbinati C, di Iasio MG, et al. Synergistic cytotoxic activity of recombinant TRAIL plus the non-genotoxic activator of the p53 pathway nutlin-3 in acute myeloid leukemia cells. *Curr Drug Metab.* 2007;8(4):395–403.
52. Ribas J, Boix J, Meijer L. (R)-roscovitine (CYC202, Seliciclib) sensitizes SH-SY5Y neuroblastoma cells to nutlin-3-induced apoptosis. *Exp Cell Res.* 2006;312(12):2394–2400.
53. Cheok CF, Dey A, Lane DP. Cyclin-dependent kinase inhibitors sensitize tumor cells to nutlin-induced apoptosis: a potent drug combination. *Mol Cancer Res.* 2007;5(11):1133–1145.
54. Kojima K, Shimanuki M, Shikami M, Andreeff M, Nakakuma H. Cyclin-dependent kinase 1 inhibitor RO-3306 enhances p53-mediated Bax activation and mitochondrial apoptosis in AML. *Cancer Sci.* 2009;100(6):1128–1136.

55. Zhu N, Gu L, Li F, Zhou M. Inhibition of the Akt/survivin pathway synergizes the antileukemia effect of nutlin-3 in acute lymphoblastic leukemia cells. *Mol Cancer Ther.* 2008;7(5):1101–1109.
56. Kojima K, Shimanuki M, Shikami M, et al. The dual PI3 kinase/mTOR inhibitor PI-103 prevents p53 induction by Mdm2 inhibition but enhances p53-mediated mitochondrial apoptosis in p53 wild-type AML. *Leukemia.* 2008;22(9):1728–1736.
57. Secchiero P, Melloni E, di Iasio MG, et al. Nutlin-3 up-regulates the expression of Notch1 in both myeloid and lymphoid leukemic cells, as part of a negative feedback antiapoptotic mechanism. *Blood.* 2009;113(18): 4300–4308.
58. Kojima K, Konopleva M, Samudio IJ, Schober WD, Bornmann WG, Andreeff M. Concomitant inhibition of MDM2 and Bcl-2 protein function synergistically induce mitochondrial apoptosis in AML. *Cell Cycle.* 2006;5(23):2778–2786.
59. Kojima K, Konopleva M, Tsao T, Nakakuma H, Andreeff M. Concomitant inhibition of Mdm2-p53 interaction and Aurora kinases activates the p53-dependent postmitotic checkpoints and synergistically induces p53-mediated mitochondrial apoptosis along with reduced endoreduplication in acute myelogenous leukemia. *Blood.* 2008;112(7): 2886–2895.
60. Tabe Y, Sebasigari D, Jin L, et al. MDM2 antagonist nutlin-3 displays antiproliferative and proapoptotic activity in mantle cell lymphoma. *Clin Cancer Res.* 2009;15(3):933–942.
61. Kojima K, Konopleva M, Samudio IJ, Ruvolo V, Andreeff M. Mitogen-activated protein kinase kinase inhibition enhances nuclear proapoptotic function of p53 in acute myelogenous leukemia cells. *Cancer Res.* 2007; 67(7):3210–3219.

Funding

Research Foundation, Flanders (Fonds Wetenschappelijk Onderzoek [FWO], G.0198.08 and G.0225.09); Cycle for Life, Belgium; Centrum voor Studie en Behandeling van Gezwelziekten, Ghent; Ghent Childhood Cancer Fund; Concerted Research Actions, UGent (Geconcerteerde Onderzoeksacties, 12051203 and 01G01307); European Community under the FP6 (project: STREP: EET-pipeline, 037260). T.V.M. is a research assistant from the FWO (011F4004). L.F. is supported by a doctoral grant from the Special Research Fund of Ghent University (011D10503). J.T. is supported by a doctoral grant from the Institute for the Promotion of Innovation through Science and Technology in Flanders (Instituut voor de Aanmoediging van Innovatie door Wetenschap en Technologie in Vlaanderen, SB/33271). I.L. is a recipient of a VIB PhD fellowship. A.R. is supported by a grant from the Emmanuel van der Schueren Foundation. M.M. and J.C. Jr are supported by the friendly society Hilfe für krebskranke Kinder Frankfurt e.V. and its foundation Frankfurter Stiftung für krebskranke Kinder.

Notes

We thank I. Rottiers for excellent technical assistance and L. Derycke for help with the mouse experiments. The sponsors had no role in the design of the study, the collection and analysis of the data, the interpretation of the results, the preparation of the manuscript, and the decision to submit the manuscript for publication.

This article presents research results of the Belgian Interuniversity Attraction Poles Program, initiated by the Belgian State, Prime Minister's Office, Science Policy Programming.

Manuscript received March 2, 2009; revised August 21, 2009; accepted September 11, 2009.